

ELECTROMAGNETIC PROBES OF DENSE MATTER IN RELATIVISTIC HEAVY-ION COLLISIONS^a

G.Q. Li, G.E. Brown, C. Gale^b

*Department of Physics and Astronomy, State University of New York
at Stony Brook, Stony Brook, NY 11793, USA*

Email: gqli@nuclear.physics.sunysb.edu

Email: popenoe@nuclear.physics.sunysb.edu

Email: gale@hendrix.physics.mcgill.ca

C.M. Ko

*Cyclotron Institute and Department of Physics, Texas A&M University,
College Station, TX 77843, USA*

Email: ko@comp.tamu.edu

Dilepton and photon production in heavy-ion collisions at SPS energies is studied in the relativistic transport model that incorporates self-consistently the change of hadron masses in dense matter. It is found that the dilepton spectra in proton-nucleus reactions can be well described by the conventional mechanisms of Dalitz decay, primary vector meson decay, decay of charmed mesons, and the initial Drell-Yan processes. However, to provide a quantitative explanation of the observed dilepton spectra in central heavy-ion collisions requires contributions other than these direct decays and also various medium effects. Introducing a decrease of vector meson masses in hot dense medium, we find that the low-mass dilepton enhancement can be satisfactorily explained. Furthermore, to explain the intermediate-mass dilepton enhancement in heavy-ion collisions, secondary processes such as $\pi a_1 \rightarrow l\bar{l}$ are found to be very important. Finally, the single photon spectra in our calculations with either free or in-medium meson masses do not exceed the upper limit measured by the WA80 Collaboration.

1 INTRODUCTION

The experimental measurement and theoretical investigation of electromagnetic observables in heavy-ion collisions constitutes one of the most active and exciting fields in physics¹. Because of their relatively weak final-state interactions with the hadronic environment, dileptons, as well as photons, are considered ideal probes of the early stage of heavy-ion collisions, where quark-gluon-plasma (QGP) formation and chiral symmetry restoration are expected^{2,3,4}.

^aBased on invited talk presented at the APCTP Workshop on Hadron Properties in Medium, in Honor of Manque Rho's 60th Birthday, Seoul, October 27-31, 1997.

^bPermanent address: Physics Department, McGill University, Montreal, QC, H3A 2T8, Canada

Dilepton mass spectra can be basically divided into three mass regions. The low-mass region below m_ϕ (~ 1 GeV) is dominated by hadronic interaction and hadronic decay in the freeze-out. In the intermediate-mass region between m_ϕ and about 2.5 GeV, the contribution from the thermalized QGP might be seen. In the high-mass region at and above $m_{J/\Psi}$ the major effort has been the detection and understanding of J/Ψ suppression.

So far, the experimental measurement of dilepton spectra in heavy-ion collisions has mainly been carried out at the CERN SPS by three collaborations: the CERES collaboration is dedicated to dielectron spectra in the low-mass region^{5,6}, the HELIOS-3⁷ collaboration has measured dimuon spectra from the its threshold up to the J/Ψ region, and the NA38/NA50⁸ collaboration measures dimuon spectra in the intermediate- and high-mass region, emphasizing the J/Ψ suppression.

Recent observation of the enhancement of low-mass dileptons in central heavy-ion collisions by the CERES^{5,6} and the HELIOS-3⁷ collaborations has generated a great deal of interest in the heavy-ion community. Different dynamical models have been used to calculate and understand these data. The results from many groups with standard scenarios (i.e., using vacuum meson properties) are in remarkable agreement with each other, but in significant disagreement with the data: the experimental spectra in the mass region from 0.3-0.6 GeV are substantially underestimated^{9,10,11,12,13,14,15,16} (see also Ref. ⁶). This has led to the suggestion of various medium effects that might be responsible for the observed enhancement. In particular, the dropping vector meson mass scenario^{9,17,18} due to the chiral symmetry restoration is found to provide a nice description of both the CERES and HELIOS-3 data. On the other hand, conventional many-body effects leading to a broadening of the rho-meson spectrum function also provide a good description of these data¹¹.

In the high-mass region around $m_{J/\Psi}$, the J/Ψ suppression has been a subject of great interest, since it was first proposed as a signal of the deconfinement phase transition¹⁹. Various investigations show that up to central S+Au collisions, the normal pre-resonance absorption in nuclear matter is sufficient to account for the observed J/Ψ suppression. However, recent data from the NA50 collaboration for central Pb+Pb collisions show an additional strong ‘anomalous’ suppression which might indicate the onset of the color deconfinement²⁰.

Enhancement of dileptons in the intermediate-mass region from about 1 GeV to about 2.5 GeV has also been observed by both the HELIOS-3 and NA38/NA50 collaborations in central S+W and S+U collisions as compared to that in the proton-induced reactions (normalized by the charged-particle multiplicity)^{7,8}. Preliminary data from the NA50 collaboration also show significant

enhancement in central Pb+Pb collisions⁸ (see also Ref. ⁶). The intermediate-mass dilepton spectra in heavy-ion collisions are particularly useful for the search of the QGP. It was originally suggested that in the intermediate-mass or the intermediate p_t region, the electromagnetic radiation from the QGP phase might shine over that from the hadronic phase^{21,22}. However, to extract from the measured dilepton spectra any information about the phase transition and the properties of the QGP, it is essential that the contributions from the hadronic phase be precisely understood and carefully subtracted.

Another piece of experimental data from CERN SPS that has been discussed extensively is the single photon spectra from the WA80 collaboration²³. In this experiment, π^0 and η spectra were measured simultaneously, so that their contributions to the single photon spectra can be subtracted. It was found that the direct photon excess over those background sources is about 5% for central S+Au collisions²³. Similar measurement of inclusive photon spectra has been carried out by the CERES collaboration²⁴. The results are very much in agreement with those of WA80, namely, the inclusive photon spectra can be basically explained by hadronic decay at the freeze-out, particular radiative decay of π^0 and η .

In various hydrodynamics calculations the absence of significant thermal photon production has been used as an indication of quark gluon plasma formation that lowers the initial temperature^{25,26}. However, there is a major uncertainty in this type of analysis, namely, the initial temperature depends sensitively on the degrees of freedom included in the analysis. Indeed, in Refs. ^{13,27}, it was found that including a sufficient amount of hadron resonances the WA80 photon data can be explained without invoking the formation of the QGP. Detailed transport model calculations²⁸ support the findings of Refs. ^{13,27}.

In this contribution, we will discuss (1) the enhancement of low-mass dileptons (Section 2), (2) the enhancement of intermediate-mass dileptons (Section 3), and (3) the lack of direct photon signal (Section 4). A brief summary and outlook is presented in Section 5.

2 Low-mass dilepton enhancement: a case for dropping rho meson mass

To calculate dilepton spectra in heavy-ion collisions and to studying possible medium effects, the relativistic transport model²⁹ based on the Walecka-type model³⁰ has been quite useful, as it provides a thermodynamically consistent description of the medium effects through the scalar and vector fields. In heavy-ion collisions at SPS energies, many hadrons are produced in the initial nucleon-

nucleon interactions. This is usually modeled by the fragmentation of strings, which are the chromoelectric flux-tubes excited from the interacting quarks. One successful model for taking into account this nonequilibrium dynamics is the RQMD model³¹. To extend the relativistic transport model to heavy-ion collisions at these energies, we have used as initial conditions the hadron abundance and distributions obtained from the string fragmentation in RQMD. Further interactions and decays of these hadrons are then taken into account as in usual relativistic transport model.

To study the effects of dropping vector meson masses^{17,18} on the dilepton spectrum in heavy-ion collisions, we have extended the Walecka model from the coupling of nucleons to scalar and vector fields to the coupling of light quarks to these fields, using the ideas of the meson-quark coupling model³². For a system of nucleons, pseudoscalar mesons, vector mesons, and axial-vector mesons at temperature T and baryon density ρ_B , the scalar field $\langle\sigma\rangle$ is determined self-consistently from

$$m_\sigma^2\langle\sigma\rangle = \frac{4g_\sigma}{(2\pi)^3} \int d\mathbf{k} \frac{m_N^*}{E_N^*} \left[\frac{1}{\exp((E_N^* - \mu_B)/T) + 1} + \frac{1}{\exp((E_N^* + \mu_B)/T) + 1} \right] \\ + \frac{0.45g_\sigma}{(2\pi)^3} \int d\mathbf{k} \frac{m_\eta^*}{E_\eta^*} \frac{1}{\exp(E_\eta^*/T) - 1} + \frac{6g_\sigma}{(2\pi)^3} \int d\mathbf{k} \frac{m_\rho^*}{E_\rho^*} \frac{1}{\exp(E_\rho^*/T) - 1} \\ + \frac{2g_\sigma}{(2\pi)^3} \int d\mathbf{k} \frac{m_\omega^*}{E_\omega^*} \frac{1}{\exp(E_\omega^*/T) - 1} + \frac{6\sqrt{2}g_\sigma}{(2\pi)^3} \int d\mathbf{k} \frac{m_{a_1}^*}{E_{a_1}^*} \frac{1}{\exp(E_{a_1}^*/T) - 1} \quad (4)$$

where we have used the constituent quark model relations for the nucleon and vector meson masses, i.e., $m_N^* = m_N - g_\sigma\langle\sigma\rangle$, $m_{\rho,\omega}^* \approx m_{\rho,\omega} - (2/3)g_\sigma\langle\sigma\rangle$, the quark structure of the η meson in free space which leads to $m_\eta^* \approx m_\eta - 0.45g_\sigma\langle\sigma\rangle$, and the Weinberg sum rule relation between the rho-meson and a_1 meson masses, i.e., $m_{a_1}^* \approx m_{a_1} - (2\sqrt{2}/3)g_\sigma\langle\sigma\rangle$.

The main contributions to dileptons with mass below 1.2 GeV are the Dalitz decay of π^0 , η and ω , the direct leptonic decay of the primary ρ^0 , ω and ϕ , the pion-pion annihilation which proceeds through the ρ^0 meson, and the kaon-antikaon annihilation that proceeds through the ϕ meson. The last two processes are unique in heavy-ion collisions, and especially the pion-pion annihilation is found to be very important for low-mass dilepton production. The explicit treatment of rho and phi meson formation, propagation, and decay in pion-pion and kaon-antikaon annihilation avoids possible double counting.

The differential widths for the Dalitz decay of π^0 , η , and ω are related to their radiative decay widths via the vector dominance model, which are taken from Ref.³³. The decay of a vector meson into the dilepton is determined by

the width,

$$\Gamma_{V \rightarrow l^+ l^-}(M) = C_{l^+ l^-} \frac{m_V^4}{3M^3} \left(1 - \frac{4m_l^2}{M^2}\right)^{1/2} \left(1 + \frac{2m_l^2}{M^2}\right). \quad (2)$$

The coefficient $C_{l^+ l^-}$ in the dielectron channel is 8.814×10^{-6} , 0.767×10^{-6} , and 1.344×10^{-6} for ρ , ω , and ϕ , respectively, and is determined from the measured width. For the dimuon channel, these values are slightly larger. The two-body processes (pion-pion and kaon-antikaon annihilation) are treated in two steps: the formation of the intermediate vector meson and its decay into dileptons.

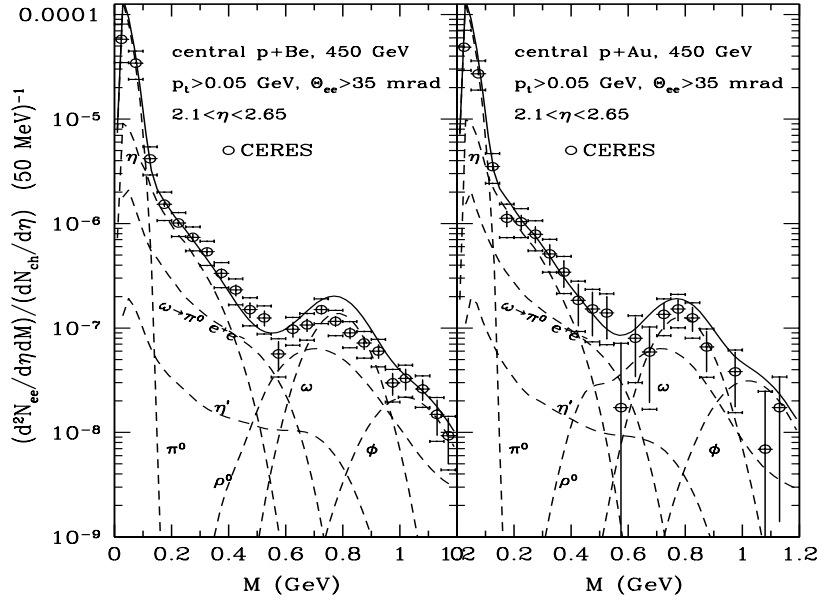


Figure 1: Dilepton invariant mass spectra in p+Be (left window) and p+Au (right window) collisions at 450 GeV.

The results for dilepton spectra from p+Be and p+Au collisions at 450 GeV are shown in Fig. 1, together with data from the CERES⁵. It is seen that the data can be well reproduced by Dalitz decay of π^0 , η and ω mesons, and direct leptonic decay of ρ^0 , ω and ϕ mesons. These results are thus similar to

those found in Ref. ¹⁰ using the Hadron-String Dynamics and those constructed by the CERES collaboration from known and expected sources of dileptons ⁵.

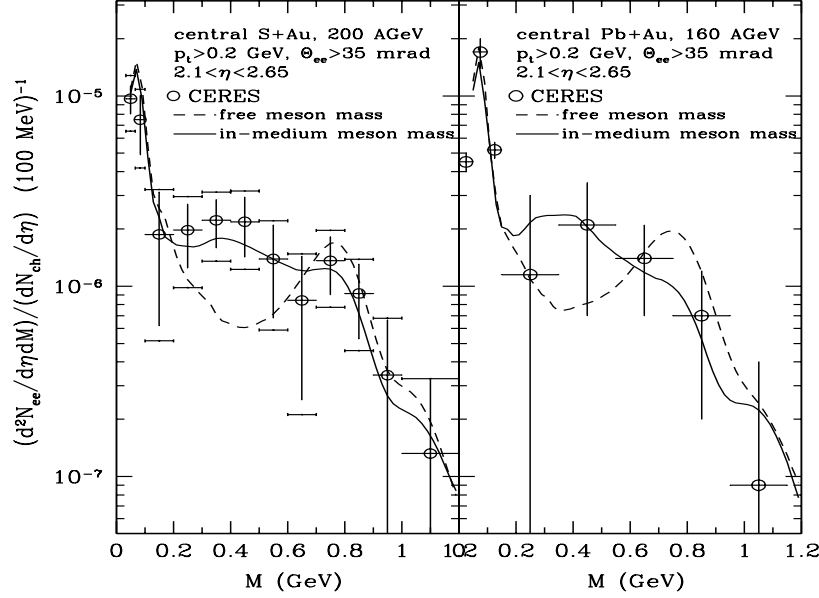


Figure 2: Dilepton invariant mass spectra in S+Au collision at 200 AGeV (left window) and Pb+Au collisions at 160 AGeV (right window). The solid and dashed curves are obtained with in-medium and free meson masses, respectively.

Our results for dilepton spectra in central S+Au collisions are shown in the left window of Fig. 2. The dashed curve is obtained with free meson masses. Although pion-pion annihilation is important for dileptons with invariant mass from 0.3 to 0.65 GeV, it still does not give enough number of dileptons in this mass region. Furthermore, for masses around $m_{\rho,\omega}$ there are more dileptons predicted by the theoretical calculations than shown in the experimental data. These are very similar to the results of Cassing *et al.* ¹⁰ based on the Hadron-String Dynamics model and Srivastava *et al.* ¹² based on the hydrodynamical model. The results obtained with in-medium meson masses are shown by the solid curve. Compared with the results obtained with free meson masses, there is about a factor of 2-3 enhancement of the dilepton yield in the mass region from 0.2 to 0.6 GeV, which thus leads to a good agreement between the

theoretical results and the CERES data. Similar conclusions that dropping vector meson masses can explain the CERES dilepton data have been obtained in Refs. ^{10,14,15}.

In the right window of Fig. 2 we compare our prediction for central Au+Pb collisions at 160 AGeV with the preliminary data from the CERES collaboration. The normalization factor $dN_{ch}/d\eta$ here is the average charge particle pseudo-rapidity density in the pseudo-rapidity range of 2 to 3, and is about 440 in this collision. In the results with free meson masses, shown by the dashed curve, there is a strong peak around $m_{\rho,\omega}$, which is dominated by ρ^0 meson decay as a result of an enhanced contribution from pion-pion annihilation in Pb+Au collisions than in S+Au and proton-nucleus collisions. In the case of in-medium meson masses, shown by the solid curve, the ρ meson peak shifts to a lower mass, and the peak around $m_{\rho,\omega}$ becomes a shoulder arising mainly from ω meson decay. At the same time we see an enhancement of low-mass dileptons in the region of 0.25-0.6 GeV as in S+Au collisions. The agreement with the data is thus significantly improved when dropping vector meson masses are used.

The same model has been used to calculate the dimuon spectra from p+W and central S+W collisions. The results for p+W are shown in the left window of Fig. 3. Again, the conventional mechanism describes quite well the measured spectra. The results for S+W collisions obtained with free meson masses are shown in the right window of Fig. 3 by the dashed curve, and are below the HELIOS-3 data in the mass region from 0.35 to 0.6 GeV, and slightly above the data around $m_{\rho,\omega}$ as in the CERES case. However, the discrepancy between the theory and the data is somewhat smaller in this case due to the smaller charged-particle multiplicity at a larger rapidity than in the CERES experiment. Our results obtained with in-medium meson masses are shown in the right window of Fig. 3 by the solid curve, and are in good agreement with the data. The importance of dropping rho meson mass in explaining the HELIOS-3 data has also been found by Cassing *et al.* ¹⁰.

It should be pointed out that, the effects of dropping rho meson mass on the low-mass dilepton spectra, as seen in Figs. 2 and 3, were predicted theoretically before the CERES data were published. In Ref. ³⁴, the RQMD model was used to calculate dilepton spectra in Au+Au collisions at AGS energies. It was found that, with an in-medium rho meson mass as predicted by the QCD sum rule calculation, the rho meson peak in the dilepton spectra shifts to about 0.5 GeV, and a significant enhancement is seen in this mass region. Similar observation was obtained in Ref. ³⁵ for dilepton spectra in heavy-ion collisions at SIS energies.

Rho meson decays dominantly into two pions. Its spectral function can

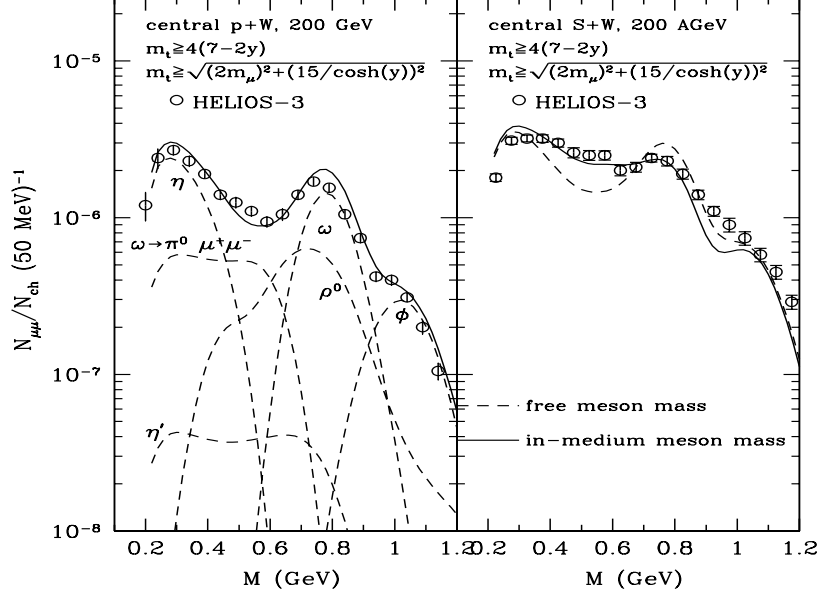


Figure 3: Dilepton invariant mass spectra in p+W (left window) and S+W (right window) collisions at 200 AGeV. In the right window the solid and dashed curves are obtained with in-medium and free meson masses, respectively.

therefore be modified by the medium modification of the pion dispersion function. Furthermore, rho meson itself can interact with nucleons to form nucleon resonances, in particular $N(1720)$ and $\Delta(1905)$, which have appreciable decay branching ratios into the ρN final state. Both effects lead to the broadening of the rho meson spectral function and thus the enhancement of low-mass dileptons from the in-medium rho meson decay. This idea was shown in Ref. ¹¹ to also lead to a reasonable description of the low-mass dilepton enhancement observed by the CERES collaboration.

3 Intermediate-mass dileptons: the importance of secondary processes

To extend the previous calculation to the intermediate mass region, we need to include additional secondary processes in addition to $\pi\pi$ and $K\bar{K}$ anni-

hilation, as well as the contributions from the charmed mesons and initial Drell-Yan processes. The last two contributions involve hard processes which scale almost linearly with the participant nucleon number, and can thus be extrapolated from the proton-proton and proton-nucleus collisions. Such a study has recently been carried out by Braun-Munzinger *et al*³⁶. The results for the central S+W collisions corresponding to the HELIOS-3 acceptance are shown in the left window of Fig. 4, which are taken from Ref. ⁶. These, together with the dileptons from the decays of primary vector mesons, are collectively labeled ‘background’. It is seen that these background sources describe very well the dimuon spectra in the p+W reactions, shown in the figure by solid circles.

However, as can be from the figure, the sum of these background sources grossly underestimates the dimuon yield in central S+W collisions, shown in the figure by open circles. Since the dimuon spectra are normalized by the measured charged particle multiplicity, this underestimation indicates additional sources to dilepton production in heavy-ion collisions. This can come from the thermalized QGP and/or hadronic phases. So the immediate next step is to check whether the contribution from the secondary hadronic processes can explain this enhancement. For dilepton spectra at low invariant masses, it is well known that the $\pi\pi$ annihilation plays an extremely important role in heavy-ion collisions. It is also expected that the other secondary processes will play a role in the dilepton spectra in the intermediate mass region.

Previous thermal rate calculations based on the kinetic theory show that in the mass and temperature region relevant for this study, the following secondary processes (from the hadronic phase) are very important: $\pi\pi \rightarrow l\bar{l}$, $\pi\rho \rightarrow l\bar{l}$, $\pi\omega \rightarrow l\bar{l}$, $\pi a_1 \rightarrow l\bar{l}$, $K\bar{K} \rightarrow l\bar{l}$, and $K\bar{K}^* + c.c \rightarrow l\bar{l}$ ^{37,38,39,40}. Among them, the $\pi a_1 \rightarrow l\bar{l}$ has been found to be the most important, mainly because of its large cross section^{38,40} (Similar conclusion has been drawn for thermal photon production^{41,42}).

We will concentrate on dilepton production from the secondary processes mentioned above. The cross sections for the annihilation of pseudoscalar mesons (P) are well known

$$\sigma_{PP \rightarrow l\bar{l}}(M) = \frac{8\pi\alpha^2 k}{3M^3} |F_P(M)|^2 \left(1 - \frac{4m_l^2}{M^2}\right) \left(1 + \frac{2m_l^2}{M^2}\right), \quad (3)$$

where k is the magnitude of the three-momentum of the pseudoscalar meson in the center-of-mass frame, M is the mass of the dilepton pair, and m_l is the mass of the lepton. It is well known that the electromagnetic form factors $|F_P(M)|^2$ play important role in these processes. The pion electromagnetic form factor is dominated by the $\rho(770)$ meson, while that of the kaon is dominated by

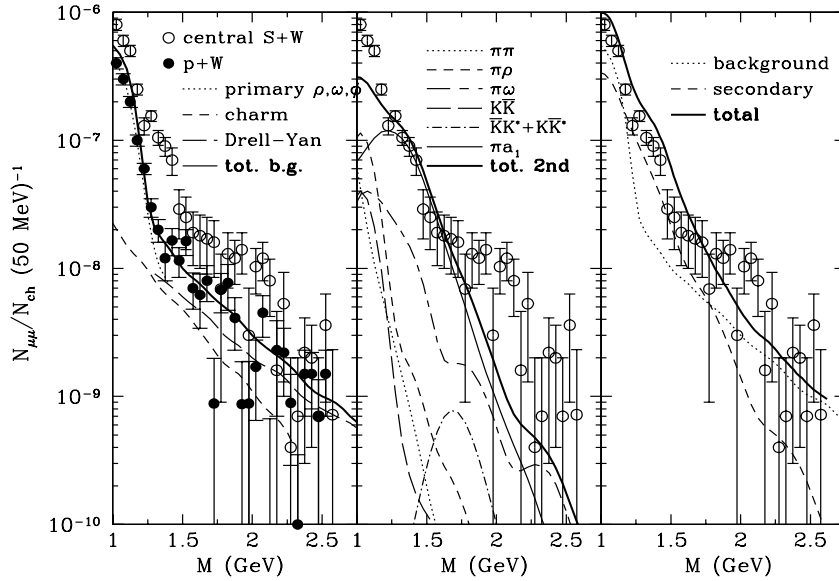


Figure 4: Left panel: comparison of backgrounds with experimental data in p+W and S+W collisions. Middle panel: contributions of various secondary processes to the dimuon spectra in central S+W collisions. Right panel: Comparison of the sum of the background and secondary contributions to the experimental data in central S+W collisions.

the phi meson. In addition, at large invariant masses, higher ρ -like resonances such as $\rho(1450)$ were found to be important⁴³.

The cross sections for $\pi\rho \rightarrow l\bar{l}$ and $\bar{K}K^* + c.c. \rightarrow l\bar{l}$, which are of the pseudoscalar-vector type, have been studied in Ref.³⁹ by fitting to the experimental data for the reverse processes (i.e., hadron production in e^+e^- annihilation)^{44,45}. High isoscalar vector mesons such as $\omega(1420)$ and $\phi(1680)$ play important roles in the electromagnetic form factors of these processes. The cross sections from Ref.³⁹ will be used in this work. The cross section for $\pi\omega \rightarrow l\bar{l}$ has the same form as that for $\pi\rho \rightarrow l\bar{l}$, but with a different form factor, which is determined from the experimental data for $e^+e^- \rightarrow \pi^0\pi^0\gamma$, as shown in Ref.⁴⁶.

The cross section for $\pi a_1 \rightarrow l\bar{l}$ needs some special attention, since this

process has been found to be particularly important in the intermediate-mass region. Already in Ref. ⁴⁰ it was shown that the dilepton production rates based on different models for the $\pi\rho a_1$ dynamics can differ by an order of magnitude. This problem was recently revisited in Ref. ⁴⁷, where a comparative study was carried out for both the on-shell properties and dilepton production rates using almost all the existing models for the $\pi\rho a_1$ dynamics. The results were indeed surprising: although most models provide reasonable description of the on-shell properties, the corresponding dilepton rate could differ by two-and-half orders of magnitude. By using the experimentally-constrained spectral function ⁴⁸, it was found that the effective chiral Lagrangian of Ref. ⁴⁹, in which the vector mesons are introduced as massive Yang-Mills fields of the chiral symmetry, provides the best off-shell, as well as on-shell, properties of the $\pi\rho a_1$ dynamics. The cross sections for $\pi a_1 \rightarrow l\bar{l}$ from this model will be used in this work.

The contributions from the secondary processes outlined above are shown in the middle panel of Fig. 4. These are obtained in the relativistic transport model of Refs. ^{9,28}, including the HELIOS-3 acceptances, mass resolution, and normalization ⁷. It is seen that the πa_1 process is by far the most important source for dimuon yields in this mass region. The $\pi\omega$ process also plays some role in the entire intermediate-mass region. The contributions from $\pi\pi$, $\pi\rho$ and $K\bar{K}$ are important around 1 GeV invariant mass.

In the right panel of Fig. 4, we add the contributions from the secondary processes obtained in our transport model to the background, and compare again with the HELIOS-3 data for central S+W collisions. It is seen that the data can now be nicely explained. Thus we showed for the first time the importance of the secondary processes for the intermediate-mass dilepton spectra in heavy-ion collisions. This is an important step forward in the use of intermediate-mass dilepton spectra as a probe of the phase transition and QGP formation. Although the current data do not show any necessity to invoke the QGP formation in S-induced reactions, consistent with conclusions from the J/Ψ physics, the observation that the secondary processes do play an important role in the intermediate-mass dilepton spectra is significant.

It is appropriate to discuss the issue of the electromagnetic form factor. While the form factors for $\pi\pi$, $\pi\rho$, $\pi\omega$, $K\bar{K}$ and $K\bar{K}^* + c.c.$ are well determined from experimental data for e^+e^- annihilation, the determination of the πa_1 electromagnetic form factor from the experimental data on $e^+e^- \rightarrow \pi^+\pi^-\pi^+\pi^-$ involves some uncertainties. In the previous calculation we assumed that all the observed 4π final state cross section proceeds through the πa_1 intermediate state. There are some indication that some of the cross section is dominated by the $\rho(1700)$ which decays directly to $\rho\pi\pi$ without going through the πa_1

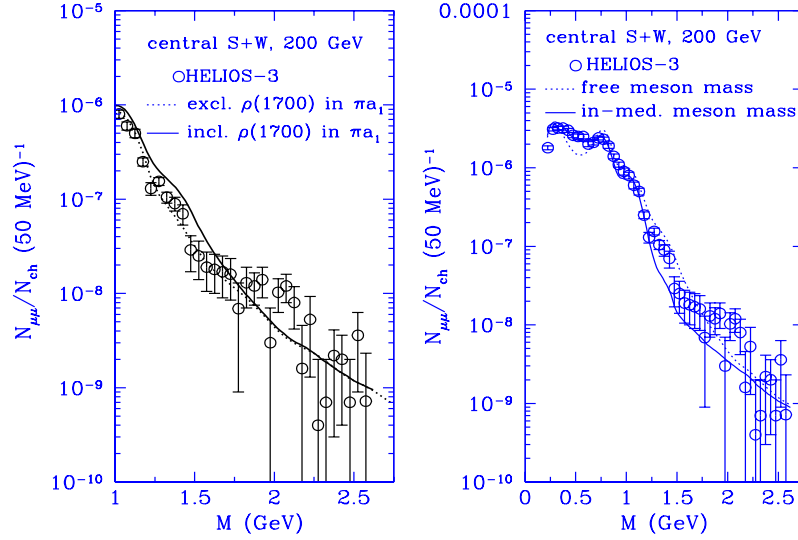


Figure 5: Left panel: comparison of dimuon spectra obtained with the full form factor and with the $\rho(700)$ only. Right panel: comparison of dimuon spectra obtained with bare and in-medium meson masses, respectively.

intermediate state⁵⁰. To see the sensitivity of our results on dimuon spectra to this uncertainty, we also did a calculation in which the πa_1 form factor contains only the normal $\rho(770)$. The cross section for $e^+e^- \rightarrow \pi a_1$ is then very similar to that obtained in Ref.⁵¹. The results are shown in the left panel of Fig. 5 by the dotted curve. Apparently, with a form factor that excludes the $\rho(1700)$ resonance, the contribution from the πa_1 process is reduced. The agreement with the HELIOS-3 data in this case is slightly better.

Another issue we want to address here is the effects of dropping vector meson masses on the entire dimuon spectra from the threshold to about 2.5 GeV. In the previous section we have shown that the enhancement of low-mass dileptons indicates that the vector meson masses decrease with increase density and temperature. This will also affect the dilepton spectra in the intermediate-mass region, through mainly two effects. One is the change of the invariant energy

spectra of these secondary meson pairs. If the rho meson mass is reduced, then the invariant energy of the $\pi\rho$ collisions should also decrease. The second effect enters through the modification of the electromagnetic form factor. Since we do know very well how the masses of the ρ -like resonances change with density and temperature, we assume that they experience the same amount of the scalar field as the ordinary rho meson, namely, $m_{\rho,\rho'}^* = m_{\rho,\rho'} - 2/3g_\sigma\langle\sigma\rangle$. The results of this calculation are shown in the right panel of Fig. 5. Below 1.1 GeV and especially from 0.4 to 0.6 GeV, the agreement with the experimental data is much better when the dropping vector meson mass scenario is introduced. At higher masses, the dropping mass scenarios somewhat underestimates the experimental data. In this mass region, however, there might be additional contributions from, e.g., secondary Drell-Yan processes⁵² that were not included in this study. Also, the issues of collisional broadening and baryon contribution need to be checked, at these invariant masses. These are under study and will be reported on later.

4 Direct photon: lack of the signal

Single photon spectra in heavy-ion collisions at CERN-SPS energies have been measured by the WA80 collaboration²³. So far, only the upper bound has been determined for the so-called ‘thermal’ photon spectra, which accounts for about 5% of the total observed single photon yield, which is dominated by neutral pion decay. In hydrodynamical calculations²⁵, the absence of significant thermal photons has been interpreted as an evidence for the formation of a quark gluon plasma. Without phase transition, the initial temperature of the hadronic gas found in Ref. ²⁵ is about 400 MeV. This leads to a large number of thermal photons from hadronic interaction which is not observed experimentally. Including the phase transition, the initial temperature is lowered to about 200 MeV²⁵, because of increased degrees of freedom. With a lower initial temperature, the thermal photon yield is thus reduced and is found to better agree with the WA80 data. However, a more recent analysis²⁷ has shown that if one includes all hadron resonances with masses below 2.5 GeV the initial temperature can also be lowered to about 200 MeV, and the WA80 photon data can then be explained without invoking the formation of a quark gluon plasma. This is basically also the conclusion of the detailed transport model analysis presented here.

For the ‘thermal’ photon spectra we include the decay of ρ , ω , η' , and a_1 mesons, as well as two-body processes such as $\pi\pi \rightarrow \rho\gamma$ and $\pi\rho \rightarrow \pi\gamma$. The decay width for $\rho \rightarrow \pi\pi\gamma$ is taken from the model of Ref. ⁵³, which describes well the measured width for $\rho^0 \rightarrow \pi\pi\gamma$. The ω and a_1 radiative decay widths

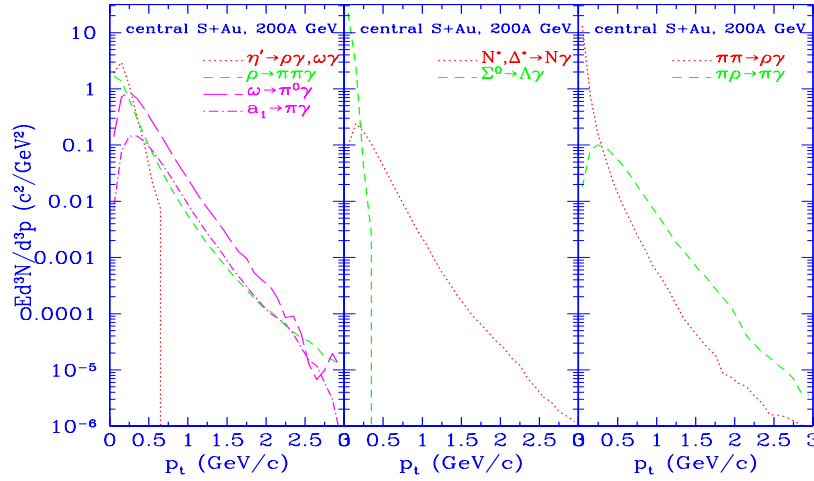


Figure 6: ‘Thermal’ photon spectra in central S+Au collisions at 200 AGeV from different sources.

are proportional to $|\mathbf{p}_\pi|$, with the coefficients determined from the measured width. For the two-body cross sections, we use the results of ²², which do not include the contribution from an intermediate a_1 meson. The latter has already been included in our model as a two-step process.

The contributions to the so-called ‘thermal’ photons from the decay of mesons and baryons, and from two-body scattering are shown in Fig. 6. The ω radiative decay is found to be the most important source for photons with transverse momenta above about 0.5 GeV. The contribution from the a_1 radiative decay is somewhat larger than that from direct $\pi\rho \rightarrow \pi\gamma$. This is in agreement with the conclusion of Ref. ⁴² that including a_1 the $\pi\rho$ contribution increases by about a factor 2-3 in the relevant temperature and photon energy region.

The contributions from η' and Σ^0 radiative decays are restricted to photons with transverse momenta below 0.5 GeV, because the mass differences between hadrons in the initial and final states in these processes are small. Photons with transverse momenta below 0.2 GeV come chiefly from the decay of Σ^0 and $\pi\pi$ scattering. The reaction $\pi\pi \rightarrow \rho\gamma$ is endothermic, with most of the available

energy going into the rho meson mass. This cross section actually diverges as the photon energy goes to zero. We have included a low-energy cut-off as in Ref. ²². The choice of this cut-off parameter affects basically only the photons with transverse momenta below about 0.1 GeV, where no experimental data are available.

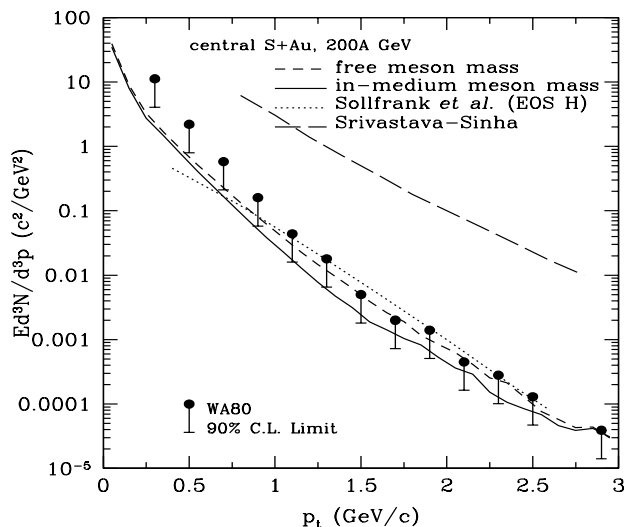


Figure 7: ‘Comparison of ‘Thermal’ photon spectra in central S+Au collisions at 200 AGeV from different calculations.

The importance of the radiative decay contribution from primary omega mesons was not seen in thermal rate calculations such as those of Ref. ²². Non-equilibrium effects and dynamical evolution of the collision attribute to the difference between the thermal and transport model calculations. As the colliding system expands, the two-body contribution becomes less important as compared with that of one-body, since the former is proportional to density squared. It was found in Ref. ²⁸ that in the first a few fm/c, when the system is the densest, the contribution from $\pi\rho$ scattering is indeed more important than that from ω decay, in agreement with the findings of the thermal rate calculation in Ref. ²². However, the rate from $\pi\rho$ damps with time very fast. After 3-5 fm/c, the emission rate from ω meson becomes more important. Adding on top of this the contribution from the omega meson decay at the

freeze out, it is easy to understand why the ω meson radiative decay becomes as important as that from $\pi\rho$ collisions in a dynamical calculation.

The WA80 single photon data have been looked at by several groups, mostly based on hydrodynamical models. In Fig. 7, we show our results together with those from¹³ and²⁵. In Ref.¹³ several different equations of state with and without quark gluon plasma formation were considered. Shown in the figure by dotted line is their results based on EOS H. This equation of state included about the same number of hadron degrees of freedom as in our transport model. It is very interesting to see that their results are very similar to ours, although the dynamical models used are quite different. In Ref.²⁵ two different equations of state, one with quark gluon plasma formation and one with pure pionic gas, were considered. Shown in the figure is their results based on the pionic gas equation of state. Because of very limited number of hadronic degrees of freedom in this equation of state, they needed a very high initial temperature to account for the final observed hadron abundances. This led to large photon yield.

5 SUMMARY AND OUTLOOK

In summary, we have studied dilepton and photon production from both proton-nucleus and nucleus-nucleus collisions using the relativistic transport model with initial conditions determined by string fragmentation from the initial stage of the RQMD model. It is found that the dilepton spectra in proton-nucleus reactions measured by the CERES and the HELIOS-3 collaboration can be well understood in terms of conventional mechanisms of Dalitz decay, direct vector meson decay, decay of charmed mesons, and initial Drell-Yan processes. For dilepton spectra in central heavy-ion collisions, these conventional mechanisms, however, fail to explain the data, in the entire mass region from threshold to about 2.5 GeV.

Including the contribution from pion-pion annihilation, which is important in the mass region from $2m_\pi$ to $m_{\rho,\omega}$, removes some of the discrepancy. But the theoretical prediction is still substantially below the data in the low mass region and somewhat above the data around $m_{\rho,\omega}$. The theoretical results are brought into good agreement with the data when reduced in-medium vector meson masses are taken into account. In the intermediate-mass region, we have included additional secondary processes involving meson-meson collisions. The cross sections for these processes are constrained by the experimental data for e^+e^- annihilation. We found that these secondary processes, especially the $\pi a_1 \rightarrow l\bar{l}$, play very important role in the intermediate-mass region. We have also calculated, within the same dynamical model, the thermal photon spectra

in central S+Au collisions. In both free meson masses and in-medium meson masses scenarios, our results do not exceed the upper limit deduced from the experiments by the WA80 collaboration.

So far, we have not included explicitly collisional broadening in our calculation. Since the rho meson is treated as a dynamical particle in our transport model, its collisions with meson (mainly pions) and baryons (mainly nucleons) are included. This might reflect, at least partly, its collisional broadening in hot and dense matter. On the other higher resonances, such as $\rho(1450)$ and $\rho(1700)$, are not treated dynamically. Their effects are included through electromagnetic form factors. Therefore, collisional broadening is not considered for these higher resonances. Since they usually have a natural width of 200-300 MeV, a collisional broadening width of about 50 MeV for these higher resonances⁵⁴ shall not affect our results dramatically. This, however, needs to be dealt with quantitatively.

The current investigation can be extended to higher incident energies, such as those of RHIC collider, by combining the cross sections (or thermal rates) obtained in this study with, e.g., hydrodynamical models for the evolution of heavy-ion collisions at the RHIC energies. This kind study will be very useful for the determination of hadronic background in the dilepton spectra, and for the clear identification of dilepton spectra from the QGP.

Acknowledgments

This work is supported in part by the U.S. Department of Energy under grant number DE-FG02-88ER-40388, by the Natural Sciences and Engineering Research Council of Canada, and by the Fonds FCAR of the Quebec Government.

References

1. For example, Quark Matter'97 *Nucl. Phys.* A590 (1995); Quark Matter'96, *Nucl. Phys.* A610 (1996).
2. E. Shuryak, *Phys. Rep.* 67 (1980) 71.
3. K. Kajantie, J. Kapusta, L. McLerran, and A. Mekjian, *Phys. Rev. D* 34 (1986) 2746.
4. G.E. Brown and M. Rho, *Phys. Rep.* 269 (1996) 333.
5. G. Agakichiev *et al.*, *Phys. Rev. Lett.* 75 (1995) 1272; J.P. Wurm for the CERES Collaboration, *Nucl. Phys.* A590 (1995) 103c; I. Tserruya, *Nucl. Phys.* A590 (1995) 127c; G. Agakichiev *et al.*, *Nucl. Phys.* A610 (1996) 317c.
6. A. Drees, *Nucl. Phys.* A610 (1996) 536c; *Nucl. Phys.* (1998), in press.

7. M. Masera for the HELIOS-3 Collaboration, *Nucl. Phys.* A590 (1995) 93c; A.L.S. Angelis, *et al* CERN-PPE/97-117.
8. M.C. Abreu *et al.*, (NA38 collaboration), *Phys. Lett. B* 368 (1996) 230; M.C. Abreu *et al.*, (NA50 collaboration), *Nucl. Phys.* A610 (1996) 331c; C. Lourenco, *Nucl. Phys.* A610 (1996) 552c.
9. G.Q. Li, C.M. Ko, and G.E. Brown, *Phys. Rev. Lett.* 75 (1995) 4007; *Nucl. Phys.* A606 (1996) 568; G.Q. Li, C.M. Ko, G.E. Brown, and H. Sorge, *ibid.* A611 (1996) 539.
10. W. Cassing, W. Ehehalt, and C. M. Ko, *Phys. Lett. B* 363 (1995) 35; W. Cassing, W. Ehehalt, and I. Kralik, *Phys. Lett. B* 377 (1996) 5.
11. G. Chanfray, R. Rapp, and J. Wambach, *Phys. Rev. Lett.* 76 (1996) 368; R. Rapp, G. Chanfray, and J. Wambach, *Nucl. Phys.* A617, 472 (1997);
12. D. K. Srivastava, B. Sinha, and C. Gale, *Phys. Rev. C* 53 (1996) R567.
13. J. Sollfrank, *et al.*, *Phys. Rev. C* 55 (1997) 392.
14. C. M. Hung and E. Shuryak, *Phys. Rev. C* 56 (1997) 453.
15. H.J. Schulze and D. Blaschke, *Phys. Lett. B* 386 (1996) 429.
16. K. Haglin, *Phys. Rev. C* 53 (1996) R2606; V. Koch and C. S. Song, *Phys. Rev. C* 54 (1996) 1903; J.V. Steele, H. Yamagishi, and I. Zahed, *Phys. Lett. B* 384 (1996) 255; R. Baier, M. Dirks, and K. Redlich, *Phys. Rev. D* 55 (1997) 4344.
17. G.E. Brown and M. Rho, *Phys. Rev. Lett.* 66 (1991) 2720.
18. T. Hatsuda and S.-H. Lee, *Phys. Rev. C* 46 (1992) R34.
19. T. Matsui and H. Satz, *Phys. Lett. B* 178 (1986) 416.
20. M.C. Abreu *et al.*, (NA50 collaboration), *Nucl. Phys.* A610 (1996) 404c; D. Kharzeev, *Nucl. Phys.* A610 (1996) 418c; C.Y. Wong, *Nucl. Phys.* A610 (1996) 434c; S. Gavin and R. Vogt, *Nucl. Phys.* A610 (1996) 442c; J.-P. Blaizot and J.-Y. Ollitrault, *Nucl. Phys.* A610 (1996) 452c.
21. E. Shuryak, *Phys. Lett. B* 79 (1978) 135.
22. J. Kapusta, P. Lichard, and D. Seibert, *Phys. Rev. D* 44 (1991) 2774.
23. R. Albrecht *et al.*, *Phys. Rev. Lett.* 76 (1996) 3506.
24. R. Baur *et al.*, *Z. Phys. C* 71 (1996) 577.
25. D. K. Srivastava and B. Sinha, *Phys. Rev. Lett.* 73 (1994) 2421.
26. A. Dumitru *et al.*, *Phys. Rev. C* 51 (1995) 2166.
27. J. Cleymans, K. Redlich, and D.K. Srivastava, *Phys. Rev. C* 55 (1997) 1431.
28. G.Q. Li and G.E. Brown, *Nucl. Phys. A*, submitted; M.A. Halasz, J.V. Steele, G.Q. Li, and G.E. Brown, nucl-th/9712006.
29. C.M. Ko and G.Q. Li, *J. Phys. G* 22 (1996) 1673.
30. B.D. Serot and J.D. Walecka, *Adv. Nucl. Phys.* 16 (1986) 1.

31. H. Sorge, H. Stöcker, and W. Greiner, *Ann. Phys.* 192 (1989) 266.
32. K. Saito and A.W. Thomas, *Phys. Rev. C* 51 (1995) 2757.
33. L. G. Landberg, *Phys. Rep.* 128 (1985) 301.
34. M. Hoffmann *et al.*, *Nucl. Phys.* A566 (1994) 15c.
35. G.Q. Li and C.M. Ko, *Nucl. Phys.* A582 (1995) 731.
36. P. Braun-Munzinger, D. Miskowiec, A. Drees, and C. Lourenco, CERN-PPE/97-65, *Z. Phys. C*, in press.
37. C. Gale and P. Lichard, *Phys. Rev. D* 49 (1994) 3338.
38. C. Song, C.M. Ko, and C. Gale, *Phys. Rev. D* 50 (1994) R1827.
39. K. Haglin and C. Gale, *Phys. Rev. D* 52 (1995) 6297.
40. J.K. Kim, P. Ko, K.Y. Lee, and S. Rudaz, *Phys. Rev. D* 53 (1996) 4787.
41. L. Xiong, E.V. Shuryak, and G.E. Brown, *Phys. Rev. D* 46 (1992) 3798.
42. C. Song, *Phys. Rev. C* 47 (1994) 3338.
43. M.E. Biagini, S. Dubnicka, E. Etin, and P. Kolar, *Nuovo Cimento A* 104 (1991) 363.
44. A. Donnachie and A.B. Clegg, *Z. Phys. C* 42 (1989) 663.
45. F. Mane *et al.*, *Phys. Lett. B* 112 (1982) 179.
46. S.I. Dolinsky *et al.*, *Phys. Rep.* 202 (1991) 99.
47. C. Gale, nucl-th/9706026; S. Gao and C. Gale, *Phys. Rev. C*, in press.
48. Z. Huang, *Phys. Lett. B* 361 (1995) 131.
49. H. Gomm, O. Kaymakcalan, and J. Schechter, *Phys. Rev. D* 30 (1984) 2345.
50. Particle Data Group, Review of Particle Properties, *Phys. Rev. D* 50 (1994) 1173.
51. G. Penso and T.N. Truong, *Phys. Lett.* 95B (1980) 143.
52. C. Spieles *et al.*, to be published.
53. P. Singer, *Phys. Rev.* 130 (1963) 2441.
54. K. Haglin, *Nucl. Phys.* A584 (1995) 719.